

Determination of spin relaxation times in heavy metals via 2nd harmonic spin injection magnetoresistance

C. Fang, C. H. Wan,* B. S. Yang, J. Y. Qin, B. S. Tao, H. Wu, X. Zhang, and X. F. Han[†]
Institute of Physics, Chinese Academy of Sciences, Beijing, 100190, China. and
University of Chinese Academy of Sciences, Beijing 100049, China.

A. Hoffmann

Material Science Division, Argonne National Laboratory, 9700 S. Cass Avenue, Lemont, IL 60439.

X. M. Liu and Z. M. Jin

Department of Physics, Shanghai University, Shanghai 200444, China.

(Dated: November 1, 2021)

Abstract: In tunnel junctions between ferromagnets and heavy elements with strong spin orbit coupling the magnetoresistance is often dominated by tunneling anisotropic magnetoresistance (TAMR). This makes conventional DC spin injection techniques impractical for determining the spin relaxation time (τ_s). Here, we show that this obstacle for measurements of τ_s can be overcome by 2nd harmonic spin-injection-magnetoresistance (SIMR). In the 2nd harmonic signal the SIMR is comparable in magnitude to TAMR, thus enabling Hanle-induced SIMR as a powerful tool to directly determine τ_s . Using this approach we determined the spin relaxation time of Pt and Ta and their temperature dependences. The spin relaxation in Pt seems to be governed by Elliott-Yafet mechanism due to a constant resistivity \times spin relaxation time product over a wide temperature range.

PACS numbers: 72.25.Rb, 72.25.Ba, 73.50.Bk, 73.40.Rw

The large applied potential of spin-orbit-torques for magnetic random access memory has stimulated intensive interest in investigating spin orbit coupling (SOC) in heavy metals such as Pt and Ta [1–11]. Their spin Hall angle (θ_{SH}), spin diffusion length (l_s) and spin relaxation time (τ_s), which influence switching efficiency are important parameters for determining their effectiveness, but especially the latter two are experimentally hard to assess. Accurate determination of τ_s could also help to identify the spin relaxation mechanisms [12]. Though θ_{SH} and l_s have been measured by spin pumping [13–17] and 2nd harmonic Hall measurement [18–20], τ_s of Pt and Ta is rarely reported. In principle, $\tau_s = l_s^2/D$, with D being the diffusion constant, which is also difficult to determine independently.

Electron spin resonance (ESR) has been a standard technique to measure the spin relaxation time of bulk light metals [21]. However, it is not suitable for ultrathin films [22, 23]. In addition, Elezzabi et al. [24] developed a time-resolved optical technique to directly measure the spin relaxation process in Au to be $\tau_{s,Au} = (45 \pm 5)$ ps. However, this method is not suitable for heavy metals such as Pt, Ta and W with short τ_s [25]. Recently, Dyakonov[26] theoretically, then Vélez et al. [27] and Wu et al. [28] experimentally demonstrated a so-called Hanle magnetoresistance (MR) effect in Pt and Ta: a spin accumulation at the sample boundaries caused by the spin Hall effect is dephased by a magnetic field via the Hanle effect, which results in an additional positive MR. This electrical method can be applied to estimate τ_s from the magnetic field dependence[27, 28]. Using this approach

$\tau_{s,Pt} = 1.9$ ps was determined for Pt/SiO₂ and 0.61 ps for Pt/YIG [28].

In fact, spin injection experiments in nonlocal spin valves [29–35] and 3-terminal geometries [36–40] are both powerful tools in measuring τ_s in metals and semiconductors. In these experiments, ferromagnetic layer (FM)/tunnel barrier/nonmagnetic layer (NM) junctions are adopted to both inject a non-equilibrium spin accumulation and simultaneously determine their magnitude. These measurement were used to determine spin relaxation times in a wide variety of materials, e.g., $\tau_{s,Si} = 55 - 285$ ps for heavily doped silicon [40]; $\tau_{s,Graphene} > 1$ ns for graphene/BN [41]; $\tau_{s,Al} = 110$ ps for aluminum [29], $\tau_{s,Cu} = 22$ ps for copper [42] and $\tau_{s,Au} = 45$ ps for gold [32].

However, it is impractical to apply these spin injection experiments to measure τ_s in heavy metals with strong SOC for at least two reasons. First, l_s in this case is so short (about several nanometers) that the preparation of nonlocal spin valves with comparable dimensions is beyond current lithography capabilities. Second, the real contact resistance is $r = r_C + r_{SI}$, where r_{SI} and r_C are the contact resistance induced by spin injection (SI) and the original contact resistance without r_{SI} , respectively. Here r_{SI} equals to $r_N r_C / (r_N + r_C)$ and the spin resistance in the NM layer r_N is defined as $\rho_N l_{sN}$. ρ_N and l_{sN} are the resistivity and spin relaxation length of NM, respectively. For this discussion we ignore the influence of spin resistance in FM on r_{SI} due to the small values of l_s in FM. Because $r_N \ll r_C$ for metals, $r \approx r_C + r_N$. As one increases a field perpendicular to the spin polarization in the NM, the spin accumulation dephases, resulting in a

vanishing r_N due to the Hanle effect. This gives rise to a $MR \equiv [r(H \rightarrow \infty) - r(0)]/r(0) = -r_N/(r_C + r_N) \approx -r_N/r_C < 0$. This negative spin-injection-induced MR (SIMR) has been utilized in 3-terminal geometries to measure τ_s in semiconductors [36–39] but is negligible in metallic systems, since $r_N \ll r_C$ by several orders of magnitude. Besides, r_C can also exhibit a field dependence due to SOC in FM/Barrier/NM junctions [43, 44]. This so-called tunneling anisotropy MR (TAMR) [45] further complicates the analysis.

In this Letter, we will show that even with a 3-terminal geometry, SIMR can be clearly observed by 2nd harmonic voltage measurements, since TAMR only dominates the 1st harmonic voltages. We adopted this method to determine τ_s in Pt and Ta and also their corresponding temperature dependences.

First we discuss the basic concept of these measurements. The tunneling conductance $g_C = 1/r_C$ is composed by counterparts for opposite spin channels, $g_C = g_{C\uparrow} + g_{C\downarrow}$. Here we have already neglected r_N in the contact resistance due to the fact that $r_N \ll r_C$. Spin

injection into the NM or spin extraction from NM induces a non-equilibrium spin accumulation μ_N in NM, which increases or decreases Fermi levels of opposite spin channels. This can further lead to a change of g_C by $\Delta g_C = \frac{dg_{C\uparrow}}{dE} \mu_N - \frac{dg_{C\downarrow}}{dE} \mu_N = \frac{d(g_{C\uparrow} - g_{C\downarrow})}{dE} \mu_N$. The spin accumulation is given by $\mu_N = pr_N j$, where p and j are the tunneling spin polarization and current density across the junction [46]. Thus $\Delta g_C = \alpha pr_N j$ with $\alpha \equiv \frac{d(g_{C\uparrow} - g_{C\downarrow})}{dE}$. The voltage across the junction $v = r_C j$ is then

$$v = \frac{1}{(g_{C,0} + \Delta g_C)} j \approx \left(\frac{1}{g_{C,0}} - \frac{\Delta g_C}{g_{C,0}^2} \right) j = \frac{1}{g_{C,0}} j - \frac{\alpha pr_N}{g_{C,0}^2} j^2 \quad (1)$$

Here $g_{C,0}$ is the contact conductance at zero current, or $v = r_{C,0} j - \alpha pr_N r_{C,0}^2 j^2$ with $r_{C,0}$ being the contact resistance at zero current. Note that $r_{C,0}$ does not contain SIMR. Assuming that $r_{C,0} = r_{C,00}(1 + \text{TAMR})$ and $r_N = r_{N,0}(1 + \text{SIMR})$, results in $v = r_{C,00}(1 + \text{TAMR})j - \alpha pr_{N,0} r_{C,00}^2 (1 + \text{SIMR})(1 + \text{TAMR})^2 j^2$, where $r_{C,00}$ and $r_{N,0}$ are the contact resistance and spin resistance at $H = 0$ and $j = 0$, respectively. This equation can be further reduced considering $\text{TAMR} \ll 1$ and $\text{SIMR} \ll 1$:

$$v \approx r_{C,00}(1 + \text{TAMR})j - \alpha pr_{N,0} r_{C,00}^2 (1 + \text{SIMR} + 2\text{TAMR})j^2 \quad (2)$$

In practice, an AC current $j = j_0 \sin(\omega t)$ satisfying $\Delta g_C < g_{C,0}/10$ was selected to make the above Taylor expansion reasonable. Thus $v_{1\omega} = r_{C,00}(1 + \text{TAMR})j_0$ has no explicit dependence on SIMR while $v_{2\omega} = \frac{1}{2}\alpha pr_{N,0} r_{C,00}^2 (1 + \text{SIMR} + 2\text{TAMR})j_0^2$ has a dependence on both SIMR and 2TAMR. They also differ in phase by 90° . We would expect that TAMR dominates in $v_{1\omega}$ while SIMR becomes comparable to the TAMR and thus observable in $v_{2\omega}$ as shown in the following experiments.

Stacks of $\text{SiO}_2/\text{Ta}(10)$ or $\text{Pt}(10)/\text{MgO}(2)/\text{Co}_{40}\text{Fe}_{40}\text{B}_{20}(4)/\text{Ta}(5)/\text{Ru}(7)$ (thickness in nm) provided by Singulus Technologies AG were deposited via magnetron-sputtering and then post-annealed with a magnetic field of 1 T along the x -axis at 300°C for 1 hour to induce an easy axis along the x -axis. M - H curves acquired by vibrating sample magnetometer (Microsense) showed in-plane magnetic anisotropy for both Ta/MgO/CoFeB and Pt/MgO/CoFeB stacks [Fig. 1(a) and (b)]. The anisotropy field of each sample is about 15 kOe along the z -axis, while the easy axis is along the x -axis. H_x smaller than 1 kOe is sufficient to align the magnetization along the easy axis.

The extended films were then processed into magnetic tunneling junctions by ultraviolet lithography and argon ion etching. The junctions had one top electrode (E1) and three bottom ones (E2, E3 and E4) [Fig. 1(c)

and (d)]. The size of the junctions was $6\ \mu\text{m} \times 6\ \mu\text{m}$. Ta/MgO/CoFeB or Pt/MgO/CoFeB junctions were surrounded by MgAlO_x for protection and also for isolating E1 from the remaining electrodes. Magnetotransport properties were measured in a physical property measurement system (Quantum Design-9T). To measure the inverse spin Hall effect (ISHE) of the bottom electrodes, an AC current with sine wave and $f = \omega/\pi = 8.7\ \text{Hz}$ was applied between E1 and E3 using a Keithley 6221 and the 1st harmonic voltage $V_{1\omega}$ between E2 and E4 was firstly pre-amplified (Stanford Research, SR560) and then picked up by a lock-in amplifier (SR830) [Fig. 1(d)].

In this setup, spin-polarized current was perpendicularly injected from the FM to the NM layer. Their spin orientation was along the x -axis at $|H_x| > 500\ \text{Oe}$. Then a voltage in the open circuit can be detected along the y -axis due to the ISHE. The field dependences of the 1st harmonic voltage $V_{1\omega}^{\text{ISHE}}$ between E2 and E4 in Ta and Pt junctions are illustrated in Fig. 1(e) and (f). The sign of $V_{1\omega}^{\text{ISHE}}$ reverses as expected with reversed sign of H_x . $V_{1\omega}^{\text{ISHE}}$ has opposite signs in the Ta and Pt due to their opposite θ_{SH} [47, 48], which indicates successful spin injection into the bottom heavy metal layer. Similar ISHE behaviors in both junctions have also been observed near room temperature. The maximum $V_{1\omega}^{\text{ISHE}}/j_0$ of Ta and Pt junctions is about 1 mΩ and 0.1 mΩ at 300 K, which is in the same order of magnitude as in Ref. [49].

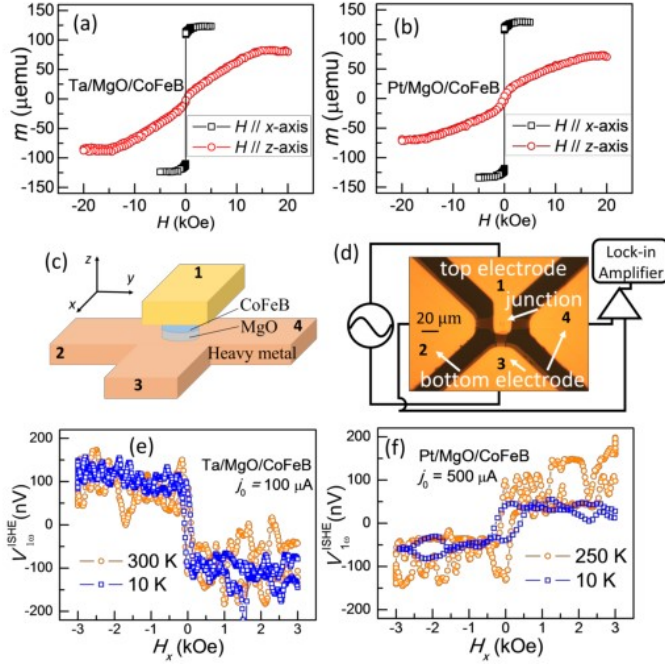


FIG. 1. (Color online) (a) and (b) Magnetic moment m vs H curve of Ta/ MgO/CoFeB and Pt/ MgO/CoFeB film. (c) Schematic of heavy metal/ MgO/Co₄₀Fe₄₀B₂₀ junctions. Top electrode 1 and bottom electrodes 2, 3 and 4 are on opposite sides of 40-nm MgAlO_x around the tunnel junction area. (d) The ISHE measurement setup applying an AC current between E1 and E3 and detecting the voltage between E2 and E4 with preamplifier and lock-in amplifier. (e) and (f) 1st harmonic ISHE voltage of Ta/ MgO/CoFeB and Pt/ MgO/CoFeB. High temperature (orange circle) or low temperature (blue) data are shown together for the Ta and Pt stacks, respectively. The current amplitude is 100 μA for Ta and 500 μA for Pt. Opposite field dependences (e) and (f) indicate different signs of θ_{SH} of Ta and Pt.

3-terminal MR measurements are further performed on both Ta and Pt junctions. We have first detected the 1st harmonic voltage $V_{1\omega}^{3T}$ between E1 and E4 with an AC current applied between E1 and E3 [inset of Fig. 2(a)]. $\text{TMR}_{1\omega}$ is defined as $[V_{1\omega}^{3T}(H) - V_{1\omega}^{3T}(0)]/V_{1\omega}^{3T}(0)$ and its field dependences is shown in Fig. 2(a)-(d). The MR originates from the tunneling junction instead of the anisotropy magnetoresistance (AMR) of the CoFeB layer. Direct measurements of AMR of the Ta and Pt showed negligible field dependence in the 1st harmonic measurements. AMR only appears in the DC measurement, whose value is negligibly small, only less than 0.05% at 10 K[50]. Except Thus, the TMR is mainly attributed to anisotropic tunneling magnetoresistance (TAMR) of the CoFeB/MgO/heavy metal junctions, and we use TAMR instead of TMR in the following analysis.

At high temperature, $\text{TAMR}_{1\omega}^z$ first quadratically increases as H_z increases from zero in both Ta and Pt junctions [Fig.2(a) and (b)] and later gradually saturates at 0.20% for Ta and 0.14% for Pt junction as H_z approaches

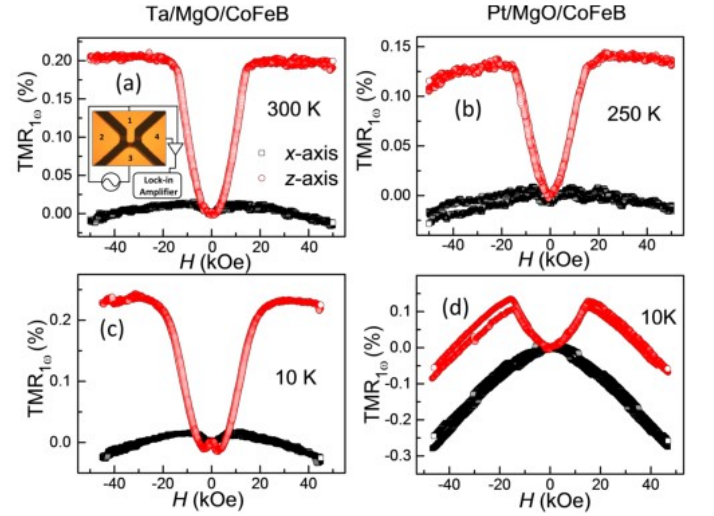


FIG. 2. (Color online) TMR obtained from 1st harmonic voltage with the 3-terminal (3T) measurement setup applying AC currents between E1 and E3 and detecting the voltages between E1 and E4 in the inset at high temperature (a) 300 K for Ta/MgO/CoFeB, (b) 250 K for Pt/MgO/CoFeB or low temperature 10 K for (c) Ta/MgO/CoFeB or (d) Pt/MgO/CoFeB. The external field is either in plane along x -axis (black square) or out of plane along z -axis (red circle). The currents are identical as in Fig. 1. (e) and (f), 100 μA for Ta/MgO/CoFeB [(a) or (c)] and 500 μA for Pt/MgO/CoFeB [(b) or (d)].

15 kOe which is also the anisotropy field of the CoFeB layer. Further increasing H_z leads to a MR reduction for both junctions. When H_x is applied, $\text{TAMR}_{1\omega}^x$ increases only by about 0.01% and then decreases gradually toward the negative MR. Note that $\text{TAMR}_{1\omega}^z$ is much larger than $\text{TAMR}_{1\omega}^x$. H_z aligns the magnetization from in-plane to out-of-plane, which subsequently changes the density of state of the interfacial FM layer via SOC and results in TAMR as predicted theoretically [45, 51]. The phenomenon $\text{TAMR}_{1\omega}^z > \text{TAMR}_{1\omega}^x$ is consistent with Ref.[52], since H_x keeps the magnetization along the easy axis, and consequently $\text{TAMR}_{1\omega}^x$ varies little.

Similar behaviors are also observed at 10 K, except for larger saturation fields and slightly larger $\text{TAMR}_{1\omega}^z$ values [Fig. 2(c) and (d)]. The negative MR, which depends on applied field instead of magnetization, is also observed at 10 K. Its origin is still unknown and beyond the scope of this study. The only remarkable difference between 10 K and high temperature is that a small negative MR (about -0.014%) appears at low H_z in the Ta junction [Fig.2(c)]. This negative MR exhibits a similar field dependence as the Hanle-effect-induced SIMR discussed below. Thus we attribute it to spin injection into Ta. This $\text{SIMR}_{1\omega}$ should have been negligibly small due to the fact $r_N \ll r_C$. In fact, it turns out to be unobservable in the Pt junction or at high temperatures. It might

be possible that inhomogeneities of the MgO layer result in a significant reduction of the effective tunneling area and smaller r_C in the Ta junction. This may lead to a reemerging of $\text{SIMR}_{1\omega}$ although $\text{SIMR}_{1\omega}$ is still one order smaller than $\text{TAMR}_{1\omega}^z$. Inhomogeneous current distribution due to the resistance of the nonmagnetic layer within the junction area could reduce the measured tunneling resistance below the real tunneling resistance by about 10.8% and 4.5% for Ta and Pt junctions respectively due to device geometry as well as inhomogeneous current distribution within the junction [53, 54]. However, this would not affect the injected spins and their dephasing process in the heavy metal layers. Therefore, this resistance adjustment would not physically influence the field dependence of the TAMR and the SIMR effects which is the basis of estimating the spin relaxation times.

$V_{2\omega}^{3T}$ was detected in the same setup as shown in the inset of Fig. 2(a). The only difference is that the 2nd harmonic voltage with 90° phase shift was measured with the lock-in amplifier. As shown in Eq. (2), SIMR should be comparable to TAMR within a factor of 2 for the 2nd harmonic signal. Thus this method renders Hanle and inverted Hanle effect signals induced by SIMR detectable even in the presence of a TAMR background (Fig.3).

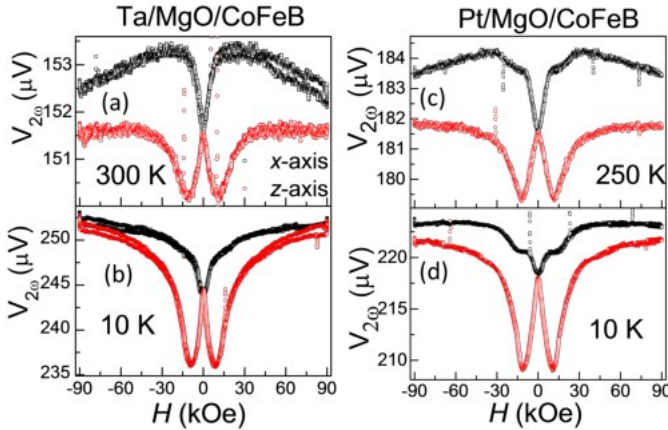


FIG. 3. (Color online) 2nd harmonic voltage with the 3-terminal (3T) measurement setup for Ta/MgO/CoFeB at (a) 300 K or (b) 10 K, and for Pt/MgO/CoFeB at (c) 250 K or (d) 10 K. The magnetic field was applied along the x -axis (black square) for inverted Hanle measurement or the z -axis (red circle) for Hanle measurement.

The field dependence of $V_{2\omega}^{3T}$ at 300 K or 250 K for Ta and Pt junction is shown in Fig. 3(a) and (b). For small H_z , the magnetization is still aligned along the easy axis. An AC current injects (extracts) spins into (from) NM and leads to a non-equilibrium spin accumulation, which conversely influences tunneling resistance and contributes an additional $V_{2\omega}$. A vertical H_z can dephase the spin accumulation via the Hanle effect and therefore diminish the additional $V_{2\omega}$, leading to a negative MR with a Lorentzian shape in the 2nd harmonic

signal. This Hanle dephasing is the same as established by Silsbee [55] for DC measurement. It is worth noting that $\text{TAMR}_{2\omega}$ and $\text{SIMR}_{2\omega}$ contribute to a positive and negative MR, respectively. In addition, $\text{TAMR}_{2\omega}$ has a H_z^2 dependence at low field according to our results in Fig. 2, while $\text{SIMR}_{2\omega}$ exhibits a Lorentzian-shape dependence. By fitting $V_{2\omega}$ vs. H_z curves with a Lorentzian function plus a H_z^2 function, we can obtain a spin relaxation time $\tau_s = e/(mB_0)$ with the electron charge e , electron mass m and B_0 being the half width at half maximum of the Lorentzian fitting. τ_s is (7.8 ± 1.6) ps at 300 K and (13.1 ± 0.6) ps at 10 K for Ta [Fig.3(a) and (b)]. By further increasing H_z beyond 10 kOe, $V_{2\omega}^{3T}$ increases due to both tilting of magnetization and the concomitant TAMR contribution.

In contrast, H_x avoids dephasing of the spin polarization along x , and therefore extends spin relaxation process and finally causes a positive MR in small field. This picture accounts for the inverted Hanle effect [40]. A similar positive SIMR also occurs for the 2nd harmonic signal (Fig.3). Besides, $V_{2\omega}$ exhibits a $H_{z/x}$ dependence at high fields, especially at 10 K, but the origin of this field dependence is unclear at this point. The Hanle signal in Fig.3 (c) and (d) results in τ_s (5.0 ± 1.5) ps at 250 K and (7.3 ± 0.6) ps at 10 K for Pt. The inverted Hanle SIMR shows similar behavior for Ta. More than 4 devices are measured to estimate the τ_s for each type of stacks. The data for the other devices are attached in the Supplementary Information[50].

In order to investigate the temperature (T) dependence of τ_s , we have conducted the 2nd harmonic SIMR measurement in a Hanle geometry at different temperatures [Fig.4(a) and (b)]. As T decreases from 300 K to 10 K, the Hanle-effect-induced $\Delta V_{2\omega}$ grows significantly by nearly one order of magnitude. In order to examine whether the field range for selecting the data affects B_0 , we have tried different ranges (± 13 kOe, ± 14 kOe and ± 15 kOe) for the fitting. The T dependence is basically the same for different fitting ranges. Their variance is less than 2 ps for both materials. Taking the ± 14 kOe fitting range, τ_s in Ta gradually decays from (13.1 ± 0.6) ps at 10 K to (7.8 ± 1.6) ps at 300 K. In contrast, if the TAMR correction is ignored in the fitting τ_s stays at 20 ps below 150 K and then decays to 14 ps at 300 K. These values are not only 50% higher than those with TAMR correction but also exhibits an unreasonable T dependence. Thus the TAMR correction is indispensable. τ_s of Pt and Ta is about 10 ps or below. These values are 1-3 orders smaller than τ_s in light metals or semiconductors, consistent with the trend that elements with larger atomic number have stronger SOC. $\tau_{s,\text{Pt}}$ is about half of $\tau_{s,\text{Ta}}$ at all temperatures in our experiment and much smaller than $\tau_{s,\text{Au}}$ of 45 ps. Here $\tau_{s,\text{Pt}} = (5.0 \pm 1.5)$ ps at 250 K is about twice of 1.9 ps measured by Hanle MR, which might be caused by lower resistivity in the former Pt and different film thickness in the two experiments.

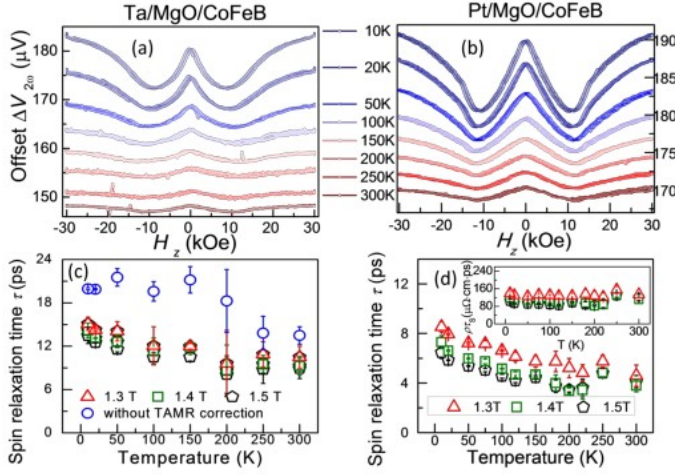


FIG. 4. (Color online) Temperature dependence of the 2nd harmonic voltage of Hanle measurements for (a) Ta/MgO/CoFeB and (b) Pt/MgO/CoFeB from 10 K to 300 K. And temperature dependence of spin relaxation time (c) for Ta/MgO/CoFeB and (d) for Pt/MgO/CoFeB acquired via fitting the data with a Lorentzian curve plus a parabolic function for the TAMR correction applied in different field ranges ± 13 Oe (red triangle), ± 14 Oe (olive square) and ± 15 Oe (black pentagon) or without the parabolic function fitting (blue circle). Inset in (d) shows that $\tau_s \rho$ remains nearly constant from 300 K to 10 K for all fitting ranges.

In our experiment, $\rho_{\text{Pt}} = 24.4 \mu\Omega\text{cm}$ at 300 K, while it is $58 \mu\Omega\text{cm}$ in Ref. [28]. $\tau_s \rho$ appears to be a constant for these two samples. The T dependence of ρ_{Pt} is also measured. For resistivity measurement, the top structure MgO/CFB/capping layers in the Pt/MgO/CFB stacks is etched away. ρ_{Pt} decreases weakly with decreasing temperature and $\tau_s \rho$ in Pt is nearly a constant from 300 K to 10 K for all the fitting ranges [inset in Fig.4(d)]. The momentum relaxation time τ_p is inversely proportional to ρ . Thus τ_s/τ_p is also a constant, which indicates that the spin relaxation in Pt is governed by Elliott-Yafet mechanism [12]. We also applied a THz technique [56] to directly measure momentum relaxation time and resistivity of Pt with 30 nm thickness, which gives $\tau_p = (5 \pm 3)$ fs and $\rho_{\text{Pt}} = 16 \mu\Omega\text{cm}$ at 300 K. Assuming that τ_p is proportional to $1/\rho_{\text{Pt}}$, τ_p in Pt/MgO/CFB is thus around 2.7 fs. Therefore the spin flip probability of each scattering τ_p/τ_s is around 7×10^{-4} for Pt at 300 K.

Our ρ_{Ta} is about $342 \mu\Omega\text{cm}$ at 300 K, much larger than those reported for the resistivity of α -phase and even β -phase Ta [57, 58], which might be due to oxidation of Ta after the top structure is etched. Therefore ρ_{Ta} vs. T is not used here for examining the spin relaxation mechanism.

In conclusion, $\text{TAMR}_{1\omega}$ dominates the 1st harmonic 3-terminal MR measurement while $\text{SIMR}_{2\omega}$ becomes significant compared to the $\text{TAMR}_{2\omega}$ background and turns out to be much easier measured in the 2nd than in the 1st

harmonic signal. This renders conventional 3-terminal FM/barrier/NM devices suitable for directly measuring the spin relaxation time τ_s of heavy metals without complications from proximity effects [59–62] that occur, when the heavy metal is in direct contact with a ferromagnet. ISHE is also observed, which proves successful spin injection into Ta and Pt. By fitting Hanle curves with a Lorentzian function plus a parabolic TAMR background, we have obtained τ_s of Ta and Pt. The τ_s for both materials exhibits a small increase from 300 K to 10 K, such that τ_s is about (7.8 ± 1.6) ps and (5.0 ± 1.5) ps for Ta and Pt at high temperature while it is about (13.1 ± 0.6) ps and (7.3 ± 0.6) ps at 10 K, respectively. Since $\tau_s \rho$ stays constant at all temperatures, the spin relaxation in Pt seems to be dominated by the Elliott-Yafet mechanism. This experimental approach provides an electrical manner to directly quantify spin relaxation time of heavy metals, which have been elusive from conventional SIMR or optical measurements. Furthermore, there is no physical limitation for this method to be generalized to other light metals and semiconductors.

ACKNOWLEDGMENTS

This work was supported by the 863 Plan Project of Ministry of Science and Technology (MOST) (Grant No. 2014AA032904), the MOST National Key Scientific Instrument and Equipment Development Projects [Grant No. 2011YQ120053], the National Natural Science Foundation of China (NSFC) [Grant No. 11434014, 51229101, 11404382] and the Strategic Priority Research Program (B) of the Chinese Academy of Sciences (CAS) [Grant No. XDB07030200]. The work from Axel Hoffmann contributing to experiment conception and data analysis was also supported by the U.S. Department of Energy, Office of Science, Basic Energy Sciences, Materials Science and Engineering Division. X. M. Liu and Z. M. Jin have contributed to THz measurement. The annealed raw films were provided by Singulus Technologies AG.

* wancaihua@iphy.ac.cn

† xfhan@iphy.ac.cn

- [1] C. O. Avci, K. Garello, I. M. Miron, G. Gaudin, S. Auffret, O. Boulle, and P. Gambardella, *Appl. Phys. Lett.* **100**, 212404 (2012).
- [2] G. Finocchio, M. Carpentieri, E. Martinez, and B. Azzerboni, *Appl. Phys. Lett.* **102**, 212410 (2013).
- [3] E. Martinez, S. Emori, and G. S. D. Beach, *Appl. Phys. Lett.* **103**, 072406 (2013).
- [4] C. H. Sim, J. C. Huang, M. Tran, and K. Eason, *Appl. Phys. Lett.* **104**, 012408 (2014).
- [5] P. V. Ong, N. Kioussis, P. K. Amiri, K. L. Wang, and G. P. Carman, *J. Appl. Phys.* **117**, 17B518 (2015).

- [6] P. M. Haney, H. W. Lee, K. J. Lee, A. Manchon, and M. D. Stiles, *Phys. Rev. B* **88**, 214417 (2013).
- [7] K. K. Meng, J. Miao, X. G. Xu, J. X. Xiao, J. H. Zhao, and Y. Jiang, *Phys. Rev. B* **93**, 060406 (2016).
- [8] S. Y. Huang, X. Fan, D. Qu, Y. P. Chen, W. G. Wang, J. Wu, T. Y. Chen, J. Q. Xiao, and C. L. Chien, *Phys. Rev. Lett.* **109**, 107204 (2012).
- [9] A. Hoffmann and S. D. Bader, *Phys. Rev. Appl.* **4**, 047001 (2015).
- [10] W. J. Kong, Y. R. Ji, X. Zhang, H. Wu, Q. T. Zhang, Z. H. Yuan, C. H. Wan, X. F. Han, T. Yu, K. Fukuda, H. Naganuma, and M. J. Tung, *Appl. Phys. Lett.* **109**, 132402 (2016).
- [11] X. Zhang, C. H. Wan, Z. H. Yuan, Q. T. Zhang, H. Wu, L. Huang, W. J. Kong, C. Fang, U. Khan, and X. F. Han, *Phys. Rev. B* **94**, 174434 (2016).
- [12] I. Žutić, J. Fabian, and S. Das Sarma, *Rev. Mod. Phys.* **76**, 323 (2004).
- [13] W. Zhang, V. Vlamincik, J. E. Pearson, R. Divan, S. D. Bader, and A. Hoffmann, *Appl. Phys. Lett.* **103**, 242414 (2013).
- [14] O. Mosendz, V. Vlamincik, J. E. Pearson, F. Y. Fradin, G. E. W. Bauer, S. D. Bader, and A. Hoffmann, *Phys. Rev. B* **82**, 214403 (2010).
- [15] V. Vlamincik, J. E. Pearson, S. D. Bader, and A. Hoffmann, *Phys. Rev. B* **88**, 064414 (2013).
- [16] O. Mosendz, J. E. Pearson, F. Y. Fradin, G. E. W. Bauer, S. D. Bader, and A. Hoffmann, *Phys. Rev. Lett.* **104**, 046601 (2010).
- [17] J. C. Rojas-Sanchez, N. Reyren, P. Laczkowski, W. Savero, J. P. Attane, C. Deranlot, M. Jamet, J. M. George, L. Vila, and H. Jaffres, *Phys. Rev. Lett.* **112**, 106602 (2014).
- [18] S. Woo, M. Mann, A. J. Tan, L. Caretta, and G. S. D. Beach, *Appl. Phys. Lett.* **105**, 212404 (2014).
- [19] Y. B. Fan, P. Upadhyaya, X. F. Kou, M. R. Lang, S. Takei, Z. X. Wang, J. S. Tang, L. He, L. T. Chang, M. Montazeri, G. Q. Yu, W. J. Jiang, T. X. Nie, R. N. Schwartz, Y. Tserkovnyak, and K. L. Wang, *Nat. Mater.* **13**, 699 (2014).
- [20] H. Reichlova, D. Kriegner, V. Holy, K. Olejnik, V. Novak, M. Yamada, K. Miura, S. Ogawa, H. Takahashi, T. Jungwirth, and J. Wunderlich, *Phys. Rev. B* **92**, 165424 (2015).
- [21] P. Monod and F. Beuneu, *Phys. Rev. B* **19**, 911 (1979).
- [22] S. Schultz and C. Latham, *Phys. Rev. Lett.* **15**, 148 (1965).
- [23] R. B. Lewis and T. R. Carver, *Phys. Rev.* **155**, 309 (1967).
- [24] A. Y. Elezzabi, M. R. Freeman, and M. Johnson, *Phys. Rev. Lett.* **77**, 3220 (1996).
- [25] P. Riego, S. Vélez, J. M. Gomez-Perez, J. A. Arregi, L. E. Hueso, F. Casanova, and A. Berger, *Appl. Phys. Lett.* **109**, 172402 (2016).
- [26] M. I. Dyakonov, *Phys. Rev. Lett.* **99**, 126601 (2007).
- [27] S. Vélez, V. N. Golovach, A. Bedoya-Pinto, M. Isasa, E. Sagasta, M. Abadia, C. Rogero, L. E. Hueso, F. S. Bergeret, and F. Casanova, *Phys. Rev. Lett.* **116**, 016603 (2016).
- [28] H. Wu, X. Zhang, C. H. Wan, B. S. Tao, L. Huang, W. J. Kong, and X. F. Han, *Phys. Rev. B* **94**, 174407 (2016).
- [29] M. Johnson and R. H. Silsbee, *Phys. Rev. Lett.* **55**, 1790 (1985).
- [30] F. J. Jedema, A. T. Filip, and B. J. van Wees, *Nature* **410**, 345 (2001).
- [31] F. J. Jedema, H. B. Heersche, A. T. Filip, J. J. A. Baselmans, and B. J. van Wees, *Nature* **416**, 713 (2002).
- [32] J. H. Ku, J. Chang, H. Kim, and J. Eom, *Appl. Phys. Lett.* **88**, 172510 (2006).
- [33] O. M. J. van't Erve, A. T. Hanbicki, M. Holub, C. H. Li, C. Awo-Affouda, P. E. Thompson, and B. T. Jonker, *Appl. Phys. Lett.* **91**, 212109 (2007).
- [34] Y. Ji, A. Hoffmann, J. S. Jiang, and S. D. Bader, *Appl. Phys. Lett.* **85**, 6218 (2004).
- [35] Y. Ji, A. Hoffmann, J. E. Pearson, and S. D. Bader, *Appl. Phys. Lett.* **88**, 052509 (2006).
- [36] S. P. Dash, S. Sharma, R. S. Patel, M. P. de Jong, and R. Jansen, *Nature* **462**, 491 (2009).
- [37] K. R. Jeon, B. C. Min, I. J. Shin, C. Y. Park, H. S. Lee, Y. H. Jo, and S. C. Shin, *Appl. Phys. Lett.* **99**, 199902 (2011).
- [38] X. Lou, C. Adelman, M. Furis, S. A. Crooker, C. J. Palmstrom, and P. A. Crowell, *Phys. Rev. Lett.* **96**, 176603 (2006).
- [39] T. Uemura, K. Kondo, J. Fujisawa, K. Matsuda, and M. Yamamoto, *Appl. Phys. Lett.* **101**, 132411 (2012).
- [40] S. P. Dash, S. Sharma, J. C. Le Breton, J. Peiro, H. Jaffres, J. M. George, A. Lemaitre, and R. Jansen, *Phys. Rev. B* **84**, 054410 (2011).
- [41] S. Singh, J. Katoch, J. S. Xu, C. Tan, T. C. Zhu, W. Amamou, J. Hone, and R. Kawakami, *Appl. Phys. Lett.* **109**, 122411 (2016).
- [42] S. Garzon, I. uti, and R. A. Webb, *Phys. Rev. Lett.* **94**, 176601 (2005).
- [43] A. Matos-Abiague and J. Fabian, *Phys. Rev. B* **79**, 155303 (2009).
- [44] O. Txoperena, M. Gobbi, A. Bedoya-Pinto, F. Golmar, X. N. Sun, L. E. Hueso, and F. Casanova, *Appl. Phys. Lett.* **102**, 192406 (2013).
- [45] C. Gould, C. Ruster, T. Jungwirth, E. Girgis, G. M. Schott, R. Giraud, K. Brunner, G. Schmidt, and L. W. Molenkamp, *Phys. Rev. Lett.* **93**, 117203 (2004).
- [46] A. Fert and H. Jaffres, *Phys. Rev. B* **64**, 184420 (2001).
- [47] C. Hahn, G. de Loubens, O. Klein, M. Viret, V. V. Naleto, and J. Ben Youssef, *Phys. Rev. B* **87**, 174417 (2013).
- [48] A. Hoffmann, *IEEE Trans. Magn.* **49**, 5172 (2013).
- [49] L. Liu, C.-T. Chen, and J. Z. Sun, *Nat. Phys.* **10**, 561 (2014).
- [50] "See Supplementary Information."
- [51] H. Saito, S. Yuasa, and K. Ando, *Phys. Rev. Lett.* **95**, 086604 (2005).
- [52] S. Hatanaka, S. Miwa, K. Matsuda, K. Nawaoka, K. Tanaka, H. Morishita, M. Goto, N. Mizuochi, T. Shinjo, and Y. Suzuki, *Appl. Phys. Lett.* **107**, 082407 (2015).
- [53] R. J. Pedersen and F. L. Vernon, *Appl. Phys. Lett.* **10**, 29 (1967).
- [54] J. S. Moodera, L. R. Kinder, J. Nowak, P. LeClair, and R. Meservey, *Appl. Phys. Lett.* **69**, 708 (1996).
- [55] M. Johnson and R. H. Silsbee, *Phys. Rev. B* **37**, 5326 (1988).
- [56] Z. M. Jin, A. Tkach, F. Casper, V. Spetter, H. Grimm, A. Thomas, T. Kampfrath, M. Bonn, M. Klau, and D. Turchinovich, *Nat. Phys.* **11**, 761 (2015).
- [57] M. H. Read and C. Altman, *Appl. Phys. Lett.* **7**, 51 (1965).
- [58] L. A. Clevenger, A. Mutscheller, J. M. E. Harper, C. Cabral, and K. Barmak, *J. Appl. Phys.* **72**, 4918

- (1992).
- [59] G. Y. Guo, Q. Niu, and N. Nagaosa, Phys. Rev. B **89**, 214406 (2014).
 - [60] J. Vogel, A. Fontaine, V. Cros, F. Petroff, J. P. Kappler, G. Krill, A. Rogalev, and J. Goulon, Phys. Rev. B **55**, 3663 (1997).
 - [61] F. Wilhelm, P. Pouloupoulos, G. Ceballos, H. Wende, K. Baberschke, P. Srivastava, D. Benea, H. Ebert, M. Angelakeris, N. K. Flevaris, D. Niarchos, A. Rogalev, and N. B. Brookes, Phys. Rev. Lett. **85**, 413 (2000).
 - [62] W. Zhang, M. B. Jungfleisch, W. J. Jiang, Y. H. Liu, J. E. Pearson, S. G. E. te Velthuis, A. Hoffmann, F. Freimuth, and Y. Mokrousov, Phys. Rev. B **91**, 115316 (2015).